Contents lists available at ScienceDirect

Plant Physiology and Biochemistry

journal homepage: http://ees.elsevier.com

Research article

Transcript profiling for regulation of sweet potato skin color in Sushu8 and its mutant Zhengshu20

Yufeng Yang [a,b,1], Dianyi Shi [c,1,**], Yannan Wang [a], Li Zhang [a], Xiangong Chen [a], Xiaoping Yang [a], Haizheng Xiong [b], Gehendra Bhattarai [b], Waltram Ravelombola [b], Dotun Olaoye [b], Guohong Yang [a,***], Ainong Shi [b,*]

[a] Cereal Crop Institute, Henan Academy of Agricultural Sciences, Zhengzhou, 450002, China
[b] Department of Horticulture, University of Arkansas, Fayetteville, AR72701, USA
[c] College of Life Sciences, Neijiang Normal University, Neijiang, 641100, China

ARTICLE INFO

Keywords
Anthocyanin metabolism
Ipomoea batatas
Skin color
WGCNA

ABSTRACT

Sweet potato [*Ipomoea batatas* (L.) Lam.] (2n = 6x = 90) is an economic important autopolyploid species and its varieties differ regarding storage root skin and flesh colors. Two sweet potato genetic lines, Sushu8 (with red skin) and its mutant Zhengshu20, which produced different colored storage roots, were used in this study. The total flavonoid, carotenoid, and anthocyanin contents of the two lines were analyzed and revealed that anthocyanin was primarily responsible for the skin color difference. In addition, the early storage root expanding stage was the key period for anthocyanin accumulation in Sushu8. A total of 24 samples, including the skins of the fibrous root and the storage root at the early and middle expanding stages as well as the flesh of the storage root at the middle expanding stage, were analyzed based on differentially expressed genes identified by transcriptome sequencing and a weighted gene co-expression network analysis. Two gene modules highly related with the regulation of sweet potato skin color through stress responses as well as starch synthesis and glucose metabolism were identified. Furthermore, the WRKY75 transcription factor gene, fructose-bisphosphate aldolase 2 gene, and other DEGs highly related to the regulation of anthocyanin metabolism were enriched in the brown and green modules.

1. Introduction

Sweet potato [*Ipomoea batatas* (L.) Lam.], a dicotyledonous hexaploid Convolvulaceae plant species (2n = 6x = 90), is an economically important crop worldwide, mainly used as food, fodder, industrial material, and an energy source (Katayama et al., 2017; Liu, 2011; Oracion et al., 1990; Yang et al., 2018). In addition to being rich in nutrients, such as starches, vitamins, and minerals, sweet potato also contains functional components in its storage roots and leaves, including carotenoids, anthocyanins, dietary fiber, and caffeoylquinic acids (Tanaka et al., 2017). Sweet potato is generally regarded as a self-incompatible crop, with varietal differences in self- and cross-incompatibilities among different genotypes (Fekadu et al., 2013). The polyploidy, large number of chromosomes, outcrossing, and vegetative propagation of sweet potato have resulted in the high heterozygosity and variability in its genetic background (Katayama et al., 2017; Liu, 2017). Because sweet potato is a clonally propagated crop, mutation breeding is effective for improving various sweet potato characteristics (Wang et al., 2007).

There are many sweet potato varieties worldwide that vary regarding storage root taste, size, shape, and skin and flesh colors. The main skin and flesh colors are white, cream, yellow, orange, pink, red, and purple (Ingabire and Hilda, 2011). Consumer acceptance of sweet potato is primarily related to the storage root appearance and taste, which are mainly influenced by biochemical components (Endrias et al., 2016; Wang et al., 2018a). Sweet potato storage root col-

Abbreviations: DEGs, differentially expressed genes; PCA, principal component analysis; WGCNA, weighted gene co-expression network analysis.

* Corresponding author.
** Corresponding author.
*** Corresponding author.
E-mail addresses: yangyiguoyyf@gmail.com (Y. Yang); onaboard@163.com (D. Shi); alman001@126.com (Y. Wang); 46493950@qq.com (L. Zhang); 254681480@qq.com (X. Chen); 34870531@qq.com (X. Yang); hxx007@email.uark.edu (H. Xiong); gb005@email.uark.edu (G. Bhattarai); wravelom@email.uark.edu (W. Ravelombola); dsolaoye@uark.edu (D. Olaoye); yangguohong9211@163.com (G. Yang); ashi@uark.edu (A. Shi)
[1] These authors contributed equally to this work.

https://doi.org/10.1016/j.plaphy.2019.12.035
Received 1 September 2019; Received in revised form 24 December 2019; Accepted 26 December 2019
Available online xxx
0981-9428/© 2019.

UNCORRECTED PROOF

ors ranging from white to orange to purple are determined based on the pigments that are produced. The two main pigments in sweet potato are carotenoids and anthocyanins, both of which are known for their antioxidant properties (Drapal et al., 2019; Teow et al., 2007; Yoshinaga et al., 1999).

In plants, anthocyanins are responsible for the red, purple, and blue coloration of tissues, but they are also important for seed dispersal and pollination, while also functioning as a feeding deterrent and protecting tissues from UV damage (Harborne and Williams, 2000; Timothy and Edwina, 1995). The anthocyanins, flavonoids, and carotenoids are the major pigments responsible for flower colors in ornamental plants (Noman et al., 2017). Anthocyanins are initially synthesized in the cytoplasm and transported to vacuoles, where they are sequestered to form colors in different plant organs (Kou et al., 2019; Zhao and Dixon, 2010). The three mechanisms proposed for the transport of anthocyanins and flavonoids involve vesicles, glutathione S-transferase, and membrane transporters (Kou et al., 2019; Zhao, 2015). Moreover, anthocyanin biosynthesis genes are regulated by the MBW complex comprising transcription factors (i.e., MYB and bHLH) and the WD40 protein (Feller et al., 2011; Gonzalez et al., 2008). The biosynthesis and accumulation of anthocyanins in plants are affected by diverse stress factors (Mahmood et al., 2016; Zhang et al., 2016). For example, previous studies confirmed that eliminating reactive oxygen species promotes anthocyanin biosynthesis and enhances drought resistance (Castellarin et al., 2007; Nakabayashi et al., 2014). Under intense light conditions, anthocyanin production is positively regulated by the NAC transcription factor ANAC078, but is negatively regulated by JUB1/ANAC042, AtNAC032, and BoNAC019 (Mahmood et al., 2016; Morishita et al., 2009; Wang et al., 2018b; Wu et al., 2012).

The skin color of purple sweet potato is due to anthocyanin accumulation. The molecular mechanism underlying the coloration of purple sweet potato has been studied by several research groups, but less attention has focused on the development of other sweet potato skin colors (Kou et al., 2019; Wang et al., 2016a, 2018a). In this study, two Chinese sweet potato genetic lines, namely Sushu8 and its mutant, Zhengshu20 were thoroughly investigated. The Sushu8 and Zhengshu20 storage root skin colors are red and yellow, respectively, but these two lines are otherwise highly similar. Group clustering based on simple sequence repeat markers verified the similarity of their genetic backgrounds (Yang et al., 2017).

Transcriptome investigation based on next-generation sequencing technology is an efficient method for gene mining, especially for crops such as sweet potato with no available reference genome. This method may also be useful for identifying differentially expressed genes (DEGs) and revealing the molecular mechanisms of sweet potato (Kou et al., 2019; Ma et al., 2016; Yang et al., 2018). In this study, RNA sequencing and a weighted gene co-expression network analysis (WGCNA) were used to examine 24 samples (four tissues or growth stages) of two sweet potato genetic lines to identify the key candidate DEGs mediating storage root skin color differences.

2. Materials and methods

2.1. Plant materials and sampling

Two Chinese sweet potato genetic lines with high yields and good qualities were used in this study, namely Sushu8 (with red skin) and its natural mutant, Zhengshu20 (with yellow skin) which obtained during field breeding (Fig. 1). The two lines were planted in greenhouse of Modern Agricultural Science and Technology Experiment Demonstration Base in Henan Academy of Agricultural Sciences, started with sweet potato vines. After rinsing in clean water to remove any adhering soil, the following four sample groups were collected in parallel for each of the two lines at 50 days after planting: (1 and 2) the skin of the fibrous root and of the storage root at the early expanding stage (storage root diameter about 0.5 cm; collected skin approximately 1 mm thick); (3) the skin of the storage root at the middle expanding stage (storage root diameter about 3 cm; collected skin approximately 1 mm thick); and (4) the flesh of the storage root at the middle expanding stage (storage root diameter about 3 cm; collected the central part of the flesh). Three biological replicates were prepared for each line and each replicate was bulked collected from five plants with equal amounts of root tissues. A total of 24 samples (2 lines x 4 sampling tissues x 3 replicates) were collected, and quickly frozen in liquid nitro-

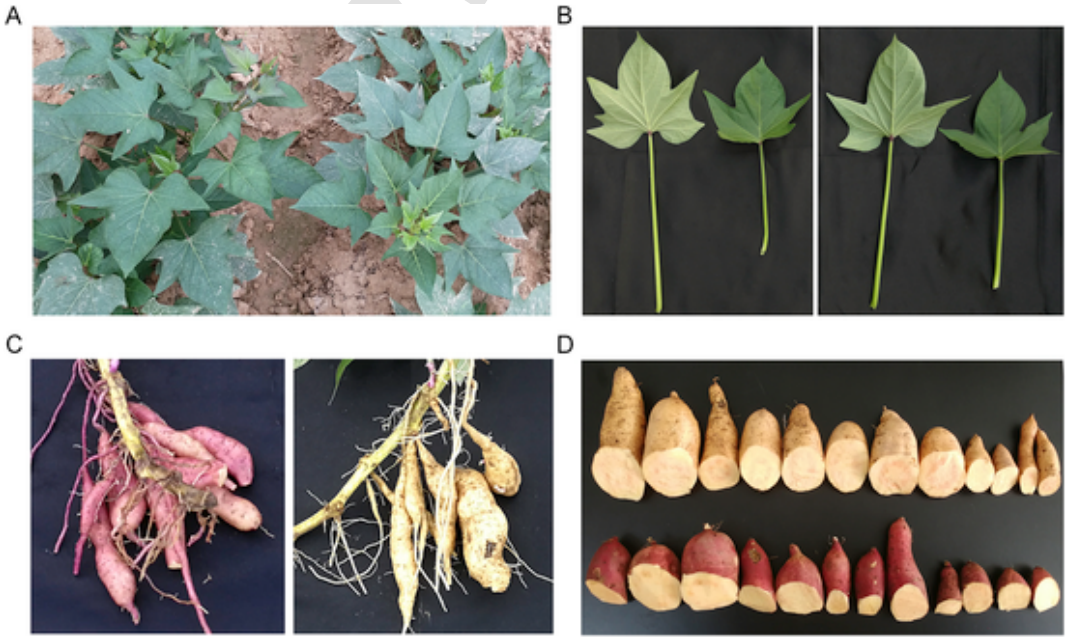

Fig. 1. Morphological characteristics of Sushu8 and Zhengshu20. (A) Appearance of Sushu8 (Left) and Zhengshu20 (Right) plants grown in the field. (B) Shape of Sushu8 (Left) and Zhengshu20 (Right) leaves. (C) Samples of Sushu8 (Left) and Zhengshu20 (Right). (D) Colors of storage root skin and flesh of Zhengshu20 (Top) and Sushu8 (Bottom). (For interpretation of the references to color in this figure legend, the reader is referred to the Web version of this article.)

gen for 5 min and then stored at −80 °C until analyzed (Table S1). Samples were similarly prepared for analyses of the total flavonoid, carotenoid, and anthocyanin contents of eight sample groups for the two genetic lines, with four biological replicates for each group.

2.2. Sequencing and raw data quality control

Total RNA was extracted with TRIzol (Thermo Fisher Scientific Inc., Waltham, Massachusetts, USA) according to the manufactures' protocol. High-quality RNA samples were used for cDNA library construction and sequencing by Genergy Biotech (Shanghai) Co., Ltd, with the Illumina HiSeq 3000 platform (Illumina Inc., San Diego, California, USA) to generate paired-end 150-bp reads. Adapter sequences and low-quality fragments were removed with the following parameters of the Skewer program (Jiang et al., 2014) (version 0.2.2): m pe, -f sanger, -l 30, -q 35, -k 8, and -Q 35. The quality of the data before and after the quality control step was assessed with the default parameters of the FastQC program (http://www.bioinformatics.babraham.ac.uk/projects/fastqc/) (version 0.11.5).

2.3. De novo transcript assembly

The fastq sequences for the data after the quality control step were used for a *de novo* sequence assembly with the Trinity program (Grabherr et al., 2011) (version 2.6.5). The multi-sample mode was applied so that all 24 samples were tab-delimited in a text file indicating the relationships among biological replicates. The following program parameters were used: -seqType fq, –SS_lib_type FR, and –min_contig_length 200. The final sequence assembly was output as a Trinity.fasta file.

2.4. Analysis of differentially expressed genes

The transcripts based on the Trinity sequence assembly were translated to proteins with the TransDecoder program (https://github.com/TransDecoder/TransDecoder/releases) (version 5.5.0). A total of 321,357 protein sequences were obtained, but after removing redundant sequences with the CD-HIT program (Li and Godzik, 2006) (version 4.7) (parameters: c 0.98 and -n 5), 96,208 protein sequences remained. The transcript sequences corresponding to the 96,208 protein sequences were selected for a subsequent gene expression analysis. After determining the transcript index with the Salmon program (Patro et al., 2017) (version 0.12.0), the gene expression levels of 24 samples were analyzed with the Salmon quant function module, with the following parameters: -libType IU and --validateMappings. Finally, the transcripts per kilobase of exon model per million mapped reads (TPM) and the number of reads mapped to each transcript (NumReads) for each gene were calculated.

The NumReads values of 24 samples were combined to screen for DEGs. The NumReads data were analyzed with the DESeq2 package (Love et al., 2014) (version 1.22.2) of the R program (version 3.5.1). Normalized NumReads values were converted with the rlog function, and the Pearson correlation coefficient was calculated with the as.matrix function. Heat maps were plotted with the heatmap.2 function of the pheatmap package (https://cran.r-project.org/web/packages/pheatmap/index.html) (version 1.0.12). A principal component analysis (PCA) was performed with the plotPCA function of DESeq2 and plotted with R. The DEGs were screened according to the following criteria: false discovery rate (i.e., adjusted p-value after multiple checks) < 0.05 and $|\log_2 \text{fold-change}| \geq 1$. The screened DEGs were compared with volcano plots and Venn diagrams that were plotted with the VennDiagram package (Chen and Boutros, 2011) (version 1.6.20) of R.

2.5. Weighted gene co-expression network analysis

The DEGs detected with DESeq2 were combined and the TPM values for the 24 samples were determined. Each TPM value was increased by 0.01 and further transformed by a $\log_{10}$ calculation. The converted data were analyzed with the R package WGCNA (Langfelder and Horvath, 2008; Zhang and Horvath, 2005) (version 1.66), with a power value of 9.

2.6. Determination of total flavonoid, carotenoid, and anthocyanin contents

The 24 samples were ground in liquid nitrogen for extraction of pigments, and spectrophotometric analysis on Multiscan GO instrument (Thermo Fisher Scientific Inc., Waltham, Massachusetts, USA) by Shanghai Sanshu Biotechnology Co., Ltd. Flavonoids were extracted with methanol as previously described method (Tian et al., 2005). An aluminum trichloride reagent was added to the extract for the complexation of the 3-hydroxyl, 4-hydroxyl, 5-hydroxyl, 4-carbonyl, or the ortho-position phenolic hydroxyl group with Al^{3+}. The resulting complex turned red under alkaline conditions, and the absorbance of the solution was measured at 510 nm. Carotenoids were extracted from ground samples with an ethanol solution containing 0.1% butylated hydroxytoluene, after which the absorbance was measured at 440 nm (Rodrigues-Amaya and Kimura, 2004). Anthocyanins were extracted from ground samples with formic acid according to Tian et al. (2005). The anthocyanins in the extract appeared red under acidic conditions, and the absorbance of the solution was measured at 520 nm.

2.7. Analysis of correlation between DEGs and total flavonoid, carotenoid, and anthocyanin contents

The correlation coefficient between TPM values of all DEGs and total flavonoid, carotenoid, and anthocyanin contents were calculated by using CORREL function in Excel to screen the DEGs underlying the differences of flavonoid, carotenoid, and anthocyanin contents. Both the top 50 positively correlated DEGs and the top 50 negatively correlated DEGs related with each pigment were screened respectively. Then, their corresponding gene connectivity ranking in the modules of WGCNA, and annotation by Arabidopsis Araport11 database according to a blastx alignment (BLAST, version 2.6.0+; set to -evalue 1e-5) were integrated for comparison.

3. Results

3.1. Quality control of sequencing data and de novo transcript assembly

An average of 56.98 M raw reads were obtained per sample, with 55.36 M clean reads obtained per sample (on average) after the quality control step. The clean reads had an average read length of 138.37 nucleotides (nt) (Table S2). An analysis of the Trinity.fasta file with the TrinityStats.pl script of the Trinity program revealed 919,584 transcripts with a GC content of 42.57%, an N50 of 1493 nt, and an average length of 832.65 nt after assembly. These transcripts corresponded to 242,218 unigenes (Table S3, Figs. S1A and B). The number of transcripts and unigenes decreased with increasing length, and the most common length was 200–500 nt. (Table S4, Figs. S1A and B). All clean data were uploaded in the NCBI Sequence Read Archive database under the BioProject PRJNA562409 with SRA accession number SRR10034756-SRR10034764.

UNCORRECTED PROOF

3.2. Pearson sample clustering and principal component analysis

The calculated Pearson correlation coefficient, which reflects the linear correlation between variables, indicated there was a high correlation between the storage root skin color in the early and middle expanding stages and the storage root flesh in the middle expanding stage, but a low correlation with fibrous roots (Table S5; Fig. S1C). The PCA transforms multiple indicators into a few comprehensive indicators by decreasing dimensionality, which simplifies complex factors to more effectively reflect data characteristics. According to the PCA results, the three biological replicates within the same group were relatively closely clustered, reflecting the high consistency among the biological replicates (Fig. S1D).

3.3. Screening for differentially expressed genes

A pairwise comparison of the gene expression levels of samples revealed relatively few DEGs between the storage root skin and flesh of each genetic line at the middle expanding stage (Table S6; Figs. S2F and H). Compared with Z4, there were 3265 DEGs in Z3. Compared with S4, there were 4591 DEGs in S3 (Table S6). A comparison with the fibrous root uncovered considerably more DEGs in each genetic line. Compared with Z1, there were 13,453 DEGs in Z3 (Table S6). Compared with S1, there were 14,368 DEGs in S3. There were substantially more downregulated DEGs than upregulated DEGs in the comparison between the storage root skin in the early or middle expanding stage and the fibrous root in the two genetic lines (e.g., Z2 versus Z1, Z3 versus Z1, S2 versus S1, and S3 versus S1) (Table S6; Figs. S2 and S3). S1, S2, S3, and S4 respectively represent the fibrous root skin, storage root skin at the early expanding stage, storage root skin at the middle expanding stage, and storage root flesh at the middle expanding stage of Sushu8; Z1, Z2, Z3, and Z4 respectively represent the fibrous root skin, storage root skin at the early expanding stage, storage root skin at the middle expanding stage, and storage root flesh at the middle expanding stage of Zhengshu20.

3.4. Weighted gene co-expression network analysis

After combining the DEGs detected with DESeq2 and removing duplicate DEGs, 29,282 DEGs were obtained. The TPM values corresponding to these DEGs for the 24 samples were used for WGCNA. On the basis of the subsequent WGCNA, the seven modules (i.e., blue, brown, green, light cyan, light green, saddle brown, and white) highly correlated with either the storage root skin and flesh or the Sushu8 and Zhengshu20 materials were selected for subsequent analyses (Fig. 2; Table 1). In each module, the DEGs based on both Cytoscape network connectivity and functions related to the regulation of sweet potato skin color in the top 20 DEGs within module were selected, and DEGs were annotated with the Araport11 *Arabidopsis thaliana* database (https://www.arabidopsis.org) according to a blastx alignment (BLAST, version 2.6.0+; set to -evalue 1e-5).

The annotations indicated that the DEGs within modules had related functions. The brown module contained some DEGs associ-

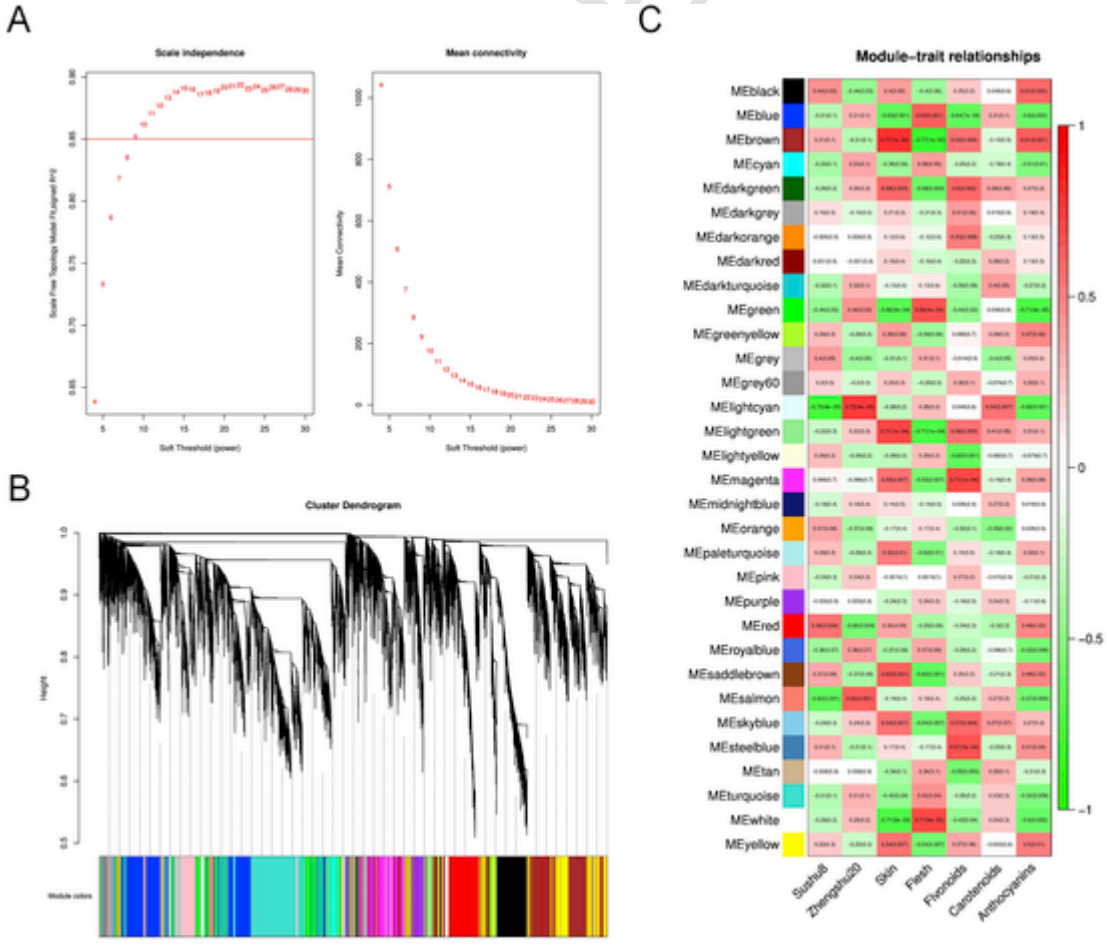

Fig. 2. WGCNA of DEGs. (A) Scale-free topology model and mean connectivity. (B) Cluster dendrogram. (C) Module-trait relationships. Variables on the x-axis are genotypes (Sushu8 and Zhengshu20), Skin, Flesh, Flavonoids, Carotenoids, and Anthocyanins. Variables on the y-axis are different modules.

Table 1
Gene Modules highly correlated with the skin color of the storage root.

Module	Skin
blue	−0.63 (0.001)
brown	0.77 (1e-0.5)
green	−0.66 (4e-04)
lightcyan	−0.28 (0.2)
lightgreen	0.71 (4e-04)
saddlebrown	0.62 (0.001)
white	−0.71 (9e-05)

ated with stress responses (Table 2). For example, AT1G16670 (Ranks 1 and 2) encodes a cold-activated plasma membrane protein kinase 1 that may phosphorylate 14-3-3 proteins (Liu et al., 2017). Additionally, AT5G14040 (Rank 3) encodes a mitochondrial phosphate transporter that regulates plant responses to salt stress. Both AT5G13080 (Rank 4) and AT1G62300 (Rank 6) encode WRKY family transcription factors. Specifically, AT5G13080 encodes the WRKY75 transcription factor, which is reportedly involved in regulating the accumulation of inorganic phosphate (Pi) and anthocyanins in plants (Lei et al., 2014). The AT1G62300 gene encodes the WRKY6 transcription factor, which contributes to the *A. thaliana* response to low-Pi stress by regulating *PHO1* expression (Chen et al., 2009). Furthermore, AT1G22180 (Rank 7) encodes a Sec14p-like phosphatidylinositol transfer family protein, which regulates the dynamic balance of phosphoinositol and intracellular protein and lipid transport in yeast (Mousley et al., 2006).

The green module included DEGs related to starch synthesis and glucose metabolism (Table 3). For example, AT4G39210 (Rank 1) encodes a glucose-1-adenosine phosphate adenylyltransferase family protein that forms the large subunit of ADP-glucose pyrophosphorylase and catalyzes the first rate-limiting step of the starch biosynthetic pathway. Moreover, AT5G48300 (Rank 2) encodes ADP-glucose pyrophosphorylase 1, which represents the small subunit of ADP-glucose pyrophosphorylase (Crevillén et al., 2005). The AT3G01180 gene (Ranks 3 and 11) encodes starch synthase 2, which affects the amylose: amylopectin ratio (Zhang et al., 2008; Patterson et al., 2018). Furthermore, AT4G38970 (Rank 4) encodes fructose-bisphosphate aldolase 2 (FBA2), which is important for plant growth (Lu et al., 2012), whereas AT5G03650 (Rank 8) encodes starch branching enzyme 2.2 (SBE 2.2), which influences amylopectin branching, thereby affecting the composition, structure, and gelatinization properties of starch (Brummell et al., 2015). The AT4G15210 gene (Rank 12) encodes the starch-degrading beta-amylase 5.

Some of the DEGs in the blue module were associated with transmembrane transport (Table 4). For example, AT4G13010 (Rank 2) encodes an oxidoreductase 2C zinc-binding dehydrogenase family protein that participates in chloroplast transmembrane transport (Curien et al., 2016). The AT1G08820 gene (Rank 5) encodes the vamp/synaptobrevin-associated protein 27-2, which may be involved in normal ER-cytoskeleton interactions and plant development (Wang et al., 2016b). Additionally, AT5G41620 (Rank 12) helps mediate the transport of vesicles from the endoplasmic reticulum to the Golgi apparatus (Noda et al., 2007). In contrast, AT5G57140 (Rank 7) encodes a purple acid phosphatase (*PAP*) gene. A previous study revealed that the overexpression of *AtPAP23* results in considerable increases in Fe and Mn contents (Zhu et al., 2005).

The heat map clustering of the hubgenes (i.e., genes with the most connections with the other genes in a module), expression barplot

Table 2
Some highly related DEGs enriched in brown module.

Gene	Rank	Connectivity	Flavonoids	Carotinoids	Anthocyanins	Arabidopsis gene	Araport11 annotation	e-value
TR139396|c1_g15_i1	1	34.92273	0.32921	−0.60831	0.385298	AT1G16670.1	Protein kinase superfamily protein	1.41E-163
TR139396|c1_g16_i1	2	34.42297	0.327384	−0.62172	0.368762	AT1G16670.1	Protein kinase superfamily protein	9.64E-123
TR102589|c1_g10_i1	3	33.64602	0.397355	−0.59242	0.601572	AT5G14040.1	phosphate transporter 3%3B1	9.90E-175
TR156288|c2_g2_i1	4	33.56723	0.385639	−0.60519	0.483593	AT5G13080.1	WRKY DNA-binding protein 75	1.04E-56
TR97258|c7_g14_i1	6	32.01261	0.338974	−0.56529	0.430169	AT1G62300.1	WRKY family transcription factor	2.61E-122
TR84256|c4_g11_i1	7	32.00228	0.495953	−0.69947	0.466891	AT1G22180.4	Sec14p-like phosphatidylinositol transfer family protein	4.48E-135

These DEGs were selected based on both Cytoscape network connectivity and functions related to the regulation of sweet potato skin color in the top 20 DEGs within module.

Table 3
Some highly related DEGs enriched in green module.

Gene	Rank	Connectivity	Flavonoids	Carotinoids	Anthocyanins	Arabidopsis gene	Araport11 annotation	e-value
TR123792|c0_g3_i1	1	36.99565	−0.54006	0.739076	−0.38402	AT4G39210.2	Glucose-1-phosphate adenylyltransferase family protein	0
TR131292|c13_g2_i2	2	36.00515	−0.53334	0.768119	−0.36353	AT5G48300.1	ADP glucose pyrophosphorylase 1	0
TR157756|c5_g4_i2	3	35.9626	−0.625	0.722598	−0.4216	AT3G01180.1	starch synthase 2	0
TR115321|c2_g2_i1	4	35.61248	−0.63019	0.417875	−0.32768	AT4G38970.1	fructose-bisphosphate aldolase 2	0
TR115420|c6_g10_i1	8	34.42375	−0.68871	0.809792	−0.35372	AT5G03650.1	starch branching enzyme 2.2	0
TR157756|c5_g5_i4	11	33.88138	−0.61143	0.713405	−0.39885	AT3G01180.1	starch synthase 2	3.13E-06
TR97098|c4_g2_i2	12	33.31581	−0.58131	0.359368	−0.32008	AT4G15210.1	beta-amylase 5	0

These DEGs were selected based on both Cytoscape network connectivity and functions related to the regulation of sweet potato skin color in the top 20 DEGs within module.

UNCORRECTED PROOF

Table 4
Some highly related DEGs enriched in blue module.

Gene	Rank	Connectivity	Flavonoids	Carotinoids	Anthocyanins	Arabidopsis gene	Araport11 annotation	e-value
TR156862|c7_g15_i1	2	36.01948	−0.11311	0.296728	−0.4434	AT4G13010.1	Oxidoreductase%2C zinc-binding dehydrogenase family protein	1.01E-149
TR156237|c0_g1_i1	5	35.12084	−0.10682	0.440621	−0.34988	AT1G08820.5	vamp/synaptobrevin-associated protein 27-2	2.81E-26
TR150361|c0_g1_i1	7	35.03601	−0.1813	0.496543	−0.45321	AT5G57140.1	purple acid phosphatase 28	2.49E-104
TR176997|c1_g8_i1	12	34.33284	−0.27324	0.537024	−0.41783	AT5G41620.4	intracellular protein transporter USO1-like protein	2.43E-130

These DEGs were selected based on both Cytoscape network connectivity and functions related to the regulation of sweet potato skin color in the top 20 DEGs within module.

of eigengene (i.e., a representative of an entire gene co-expression module) and the TPM histogram indicated that in the brown module, gene expression levels were relatively high in the fibrous root of Sushu8, but decreased in the storage root skin in the early and middle expanding stages and in the flesh during the middle expanding stage (Fig. 3A and B). The gene expression levels in the brown module exhibited similar trends in Zhengshu20 and Sushu8, but the expression levels in each tissue were lower in Zhengshu20 than in Sushu8 (Fig. 3A, B and S4

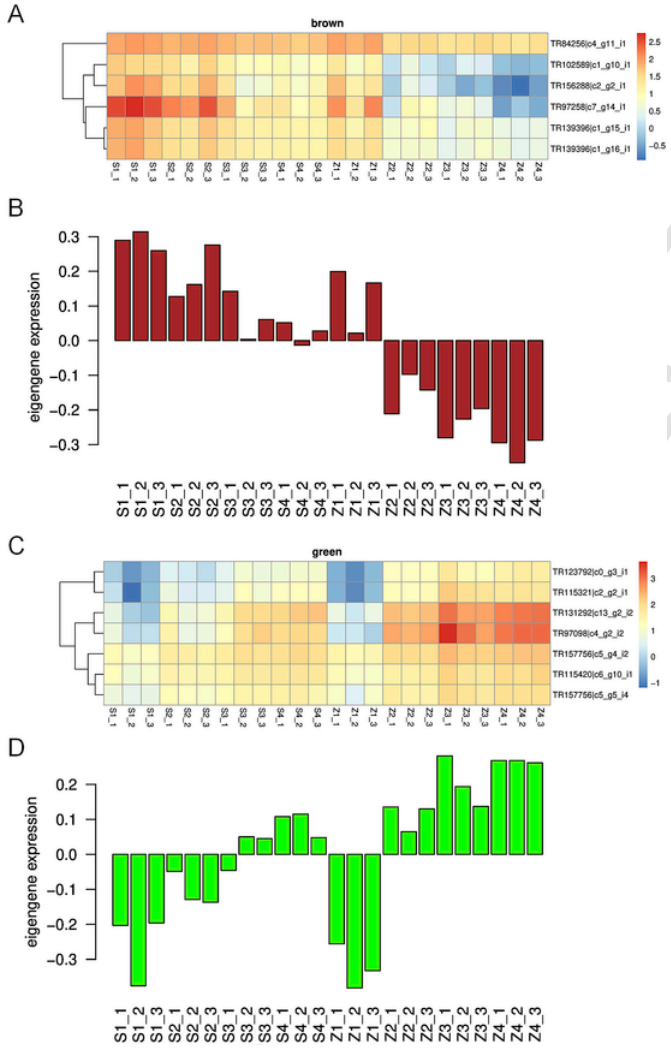

Fig. 3. Heat map clustering of hubgenes and expression barplot of eigengene enriched in the brown module (A, B) and green module (C, D). (For interpretation of the references to color in this figure legend, the reader is referred to the Web version of this article.)

). The hub gene expression levels in the green module exhibited the opposite trend to those in the brown module, with low expression levels in the fibrous root, but increased expression levels in the storage root skin in the early and middle expanding stages as well as in the flesh during the middle expanding stage (Fig. 3C and D). A comparison of the tissue types between Zhengshu20 and Sushu8 proved that the gene expression levels were higher in Zhengshu20 (Fig. 3C, D and S5).

3.5. Determination of total flavonoid, carotenoid, and anthocyanin contents

Small differences were detected in the total flavonoid and carotenoid contents in the fibrous root and the storage root skin in the early expanding stage of Sushu8 and Zhengshu20 (Fig. 4A and B; Table 5). There was a significant difference in the total flavonoid content between Sushu8 and Zhengshu20 in the storage root skin during the middle expanding stage (Fig. 4A; Table 5). Additionally, Zhengshu20 accumulated more total carotenoids than Sushu8 in the flesh during the middle expanding stage (Fig. 4B; Table 5). An analysis of the total anthocyanin content revealed significant differences between Sushu8 and Zhengshu20 in the fibrous root, and even larger differences between the two genetic lines in the storage root skin during the early expanding stage (Fig. 4C; Table 5). There was a significant difference between Sushu8 and Zhengshu20 regarding the total anthocyanin content in the storage root skin during the middle expanding stage, but the trend was lower than that during the early expanding stage (Fig. 4C). In the storage root flesh during the middle expanding stage, there was no significant difference in the total anthocyanin content between Sushu8 and Zhengshu20 (Fig. 4C; Table 5).

3.6. Analysis of correlation between DEGs and total flavonoid, carotenoid, and anthocyanin contents

The integrated results of top 50 DEGs with high correlation coefficient with each pigment, gene connectivity ranking in the modules of WGCNA, and annotation by Arabidopsis Araport11 database were compared. Within the top 50 positively correlated DEGs with flavonoids, 9 DEGs are enriched in brown module by WGCNA (Table S7). Within the top 50 negatively correlated DEGs with flavonoids, 28 and 2 DEGs are respectively enriched in green and blue modules by WGCNA (Table S8). Within the top 50 positively correlated DEGs with carotenoids, 19 and 4 DEGs are respectively enriched in green and blue modules by WGCNA (Table S9). Within the top 50 negatively correlated DEGs with carotenoids, 22 DEGs are enriched in brown module by WGCNA (Table S10). Within the top 50 positively correlated DEGs with anthocyanins, 30 DEGs are enriched in brown module by WGCNA (Table S11). Within the top 50 negatively correlated DEGs with anthocyanins, 29 and 8 DEGs are respectively enriched in blue and green modules by WGCNA (Table S12).

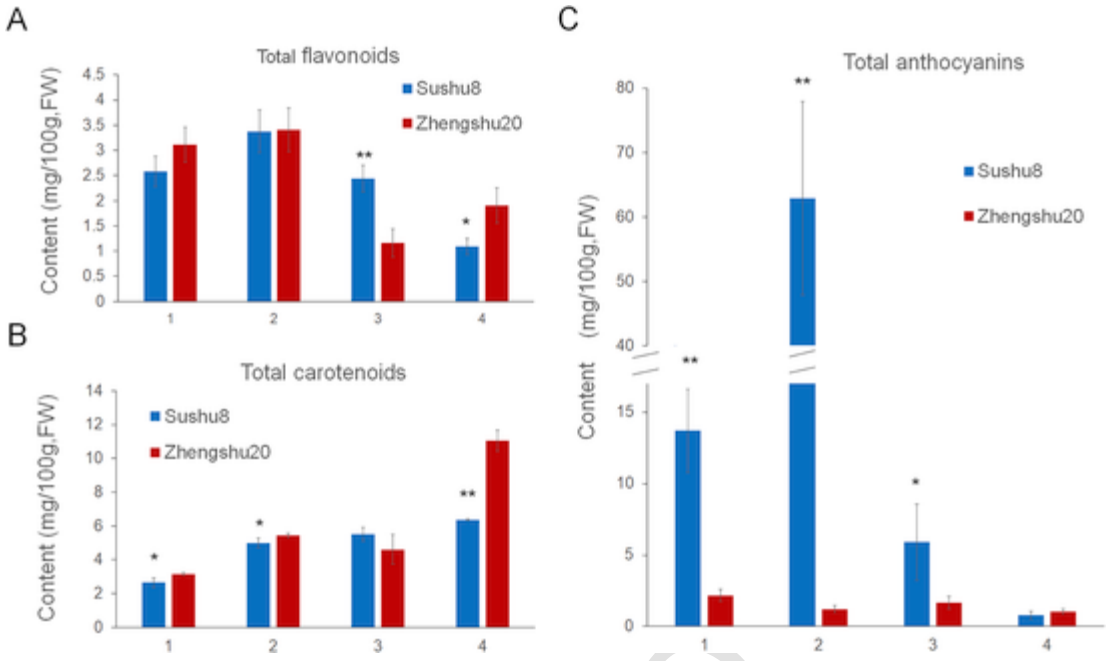

Fig. 4. Histogram of the total flavonoid (A), carotenoid (B), and anthocyanin (C) contents. Asterisks indicate a significant difference compared with Zhengshu20 contents at *P < 0.05 or **P < 0.01 (*t*-test). 1, 2, 3, and 4 respectively represent the fibrous root skin, storage root skin at the early expanding stage, storage root skin at the middle expanding stage, and storage root flesh at the middle expanding stage.

Table 5
Total flavonoid, carotenoid and anthocyanin contents (mg/100 g fresh weight).

Sample	Total flavonoids	Total carotenoids	Total anthocyanins
S1	2.58 ± 0.30 (9.67E-02)	2.65 ± 0.28 (2.58E-02 *)	13.70 ± 2.92 (5.10E-04 **)
S2	3.38 ± 0.43 (9.27E-01)	5.00 ± 0.28 (4.82E-02 *)	62.85 ± 15.03 (9.59E-04 **)
S3	2.44 ± 0.27 (1.32E-03 **)	5.52 ± 0.41 (1.61E-01)	5.90 ± 2.68 (3.52E-02 *)
S4	1.09 ± 0.16 (1.44E-02 *)	6.36 ± 0.06 (1.18E-05 **)	0.78 ± 0.26 (2.19E-01)
Z1	3.11 ± 0.35	3.15 ± 0.10	2.17 ± 0.42
Z2	3.41 ± 0.43	5.43 ± 0.14	1.22 ± 0.24
Z3	1.16 ± 0.28	4.61 ± 0.89	1.66 ± 0.43
Z4	1.91 ± 0.35	11.04 ± 0.61	1.04 ± 0.20

S1, S2, S3, and S4 respectively represent the fibrous root skin, storage root skin at the early expanding stage, storage root skin at the middle expanding stage, and storage root flesh at the middle expanding stage of Sushu8. Z1, Z2, Z3, and Z4 respectively represent the fibrous root skin, storage root skin at the early expanding stage, storage root skin at the middle expanding stage, and storage root flesh at the middle expanding stage of Zhengshu20. Asterisks indicate a significant difference compared with Zhengshu20 contents at *P < 0.05 or **P < 0.01 (*t*-test).

4. Discussion

There are many sweet potato varieties worldwide, which vary in terms of storage root skin and flesh colors. The two main pigments responsible for these color differences in sweet potato are carotenoids and anthocyanins (Drapal et al., 2019; Wang et al., 2018a). The total flavonoid, carotenoid, and anthocyanin contents of Sushu8 and Zhengshu20 were measured and the results showed that the anthocyanin was the main pigment causing the storage root skin color differences (Fig. 4; Table 5). A previous study of potato flesh color indicated that anthocyanin contents were as high as 78 mg/100 g fresh weight in growing tubers, but only 10–39 mg/100 g fresh weight in fully mature tubers (Šulc et al., 2017). Similarly, our data revealed that the early storage root expanding stage was the key period for anthocyanin accumulation. The accumulation and stability of anthocyanins are affected by various environmental conditions, including light, temperature, water stress, and pH, as well as by mechanical injuries and pathogen infections (Lin-Wang et al., 2011; Liu et al., 2019; Velu et al., 2016). In *A. thaliana*, high temperatures decrease anthocyanin accumulation and the expression of the genes in the anthocyanin biosynthetic pathway (Kim et al., 2017), whereas low temperatures increase the anthocyanin content (Leyva et al., 1995). In apple, anthocyanin biosynthesis is inhibited at high temperatures, which is accompanied by the downregulated expression of the genes in the anthocyanin biosynthetic pathway (Lin-Wang et al., 2011). In tomato, transcription factors S1AN2, S1AN1, and S1JAF13 mediate anthocyanin biosynthesis at low temperatures (Kiferle et al., 2015; Qiu et al., 2016). In potato, high temperatures significantly decrease the anthocyanin content in tubers. A study by Liu et al. (2019) proved that StMYB44 regulates anthocyanin biosynthesis in potato flesh at high temperatures.

In this study, 29,282 DEGs were detected by a pairwise comparison of eight sample groups with the DESeq2 software. After a WGCNA of the DEGs, seven modules with DEGs highly correlated with either the storage root skin and flesh colors or the Sushu8 and Zhengshu20 materials were obtained (Fig. 2; Table 1). The DEGs related to the regulation of sweet potato skin color in top 20 DEGs based on Cytoscape network connectivity in the brown, green, and blue modules were functionally annotated (Tables 2–4). By comparision, we further found that many of the highly correlated DEGs obtained by Excel CORREL function are highly coincident with the brown, green, and blue modules obtained from WGCNA, suggesting the reliability of WGCNA. Although most of the highly correlated DEGs obtained by Excel CORREL function are ranked lower in the modules, they showed some certain patterns (Tables 2–4). For example, in the brown module, all the 6 DEGs are positively correlated with flavonoids and anthocyanins, but negatively correlated with carotenoids (Table 2). In contrast to the brown module, the green module showed opposite trend that all the 7 DEGs were negatively correlated with flavonoids and anthocyanins, but positively correlated with carotenoids (Table 3). The trend of the blue module is similar to that of the green module, but the absolute value

UNCORRECTED

of correlation coefficient between the 4 DEGs and flavonoids are smaller (Table 4).

In the brown module, AT1G16670 (Ranks 1 and 2) encodes a cold-activated plasma membrane protein kinase that may phosphorylate the 14-3-3 proteins. The phosphorylated 14-3-3 proteins are shuttled from the cytosol to the nucleus, where they interact with and regulate the stability of the key cold-response C-repeat-binding factor proteins, thereby influencing the response to cold stress (Liu et al., 2017). Some studies confirmed that temperature particularly affects anthocyanin metabolism in diverse plant species (Kiferle et al., 2015; Kim et al., 2017; Leyva et al., 1995;Lin-Wang et al., 2011; Liu et al., 2019; Qiu et al., 2016). The AT5G13080 (Rank 4) and AT1G62300 (Rank 6) DEGs respectively encode important WRKY family transcription factors WRKY75 and WRKY6, which is reportedly involved in regulating root development and responses to insufficient nutrient availability. The WRKY75 transcription factor is an important component of Pi stress responses and a positive regulator of many phosphate starvation-induced genes. Anthocyanins accumulate under Pi starvation conditions, with WRKY75 considerably mediating the accumulation and absorption of anthocyanins in plants (Devaiah and Raghothama, 2007a; Devaiah et al., 2007b). Additionally, WRKY6 is involved in the response of *A. thaliana* to low-Pi stress by regulating *PHO1* expression. The regulation of *PHO1* by WRKY6 is dependent on Pi, and an exposure to low Pi conditions can release the inhibition of *PHO1* expression, possibly via proteolysis mediated by the 26S proteasome (Chen et al., 2009). Moreover, conserved WRKY-based regulatory mechanisms contribute to the *A. thaliana* proanthocyanidin pathway and the petunia anthocyanin pathway (Lloyd et al., 2017; Verweij et al., 2016). Verweij et al. (2016) proposed a model in which the petunia MBW complex activates *PH3* expression. The PH3 WRKY factor then combines with the MBW complex to target the expression of *PH1* and *PH5*, resulting in the acidification of vacuoles to modify flower colors. Our results suggest that both cold response-related genes and WRKY transcription factors may promote the anthocyanin accumulation in the sweet potato storage root skin.

In the green module, AT4G39210 (Rank 1) and AT5G48300 (Rank 2) encode the large and small subunits of ADP-glucose pyrophosphorylase, respectively. The large subunit (ApL) plays a regulatory role, and ApL3 is the major large subunit type in the inflorescence, fruit, and root. The small subunit (ApS) has a catalytic role, and ApS1 is the main small subunit type in plant tissues (Crevillén et al., 2005). The AT3G01180 gene (Ranks 3 and 11) encodes starch synthase 2, which is an important enzyme for the starch synthesis in leaves because it extends the intermediate-length glucan chains (Patterson et al., 2018; Zhang et al., 2008). Moreover, AT5G03650 (Rank 8) encodes the SBE2.2. In cassava, *SBE2.2* is highly expressed in the leaves, stem cortex, and root stele, and is increasingly expressed in growing storage roots, suggesting that it may be important for the starch biosynthetic pathway (Pei et al., 2015). Furthermore, AT4G38970 (Rank 4) encodes FBA2, which is a crucial enzyme in plants because of its functions associated with glycolysis and gluconeogenesis in the cytoplasm and the Calvin cycle in plastids (Lu et al., 2012).

Starch accumulates in chloroplasts during the day and is degraded to sugars at night when photosynthesis is not active (Zeeman et al., 2010). In plants, the regulation of sugar levels is not only due to simple metabolic effects or osmotic pressure because sugars also serve as signaling molecules and exhibit hormone-like signal transduction functions (Moore et al., 2003). In *A. thaliana*, the upregulation of the anthocyanin biosynthetic pathway is dependent on sucrose. The expression levels of several genes, including *C4H*, *CHS*, *CHI*, *F3H*, *F3′H*, *FLS*, *DFR*, *LDOS*, *UF3GT*, and *MYB75/PAP1* (transcription factor genes), are reportedly regulated by sucrose (Solfanelli et al., 2006; Teng et al., 2005). Zheng et al. (2009) previously confirmed that grape berries were most sensitive to sugars at 70 days after flowering, suggesting that sugar may induce anthocyanin accumulation in grape berries through a hexokinase-dependent pathway. A proteome-level investigation by Wang et al. (2016a) proved that 40% of the identified differentially expressed proteins were involved in the starch metabolism and glycolysis related to the synthesis of anthocyanin precursors. Moreover, the starch in purple sweet potato might be degraded to glucose-1-phosphate, which then enters the glycolytic and shikimate pathways to produce anthocyanin precursors. Our results suggest that glucose metabolism may be involved in the anthocyanin accumulation in the sweet potato storage root.

5. Conclusions

The data presented herein revealed that anthocyanin was the main pigment responsible for the color differences between Sushu8 and Zhengshu20. Additionally, the early storage root expanding stage was the key period for anthocyanin accumulation in Sushu8. Two gene modules (i.e., brown and green modules) related to stress responses, starch synthesis, and glucose metabolism were screened based on a DEG analysis and WGCNA after a transcriptome sequencing step. Moreover, *WRKY75* (AT5G13080), *FBA2* (AT4G38970), and other DEGs highly related to the regulation of anthocyanin metabolism were enriched in the two modules.

Contribution

Yufeng Yang and Dianyi Shi designed this study and did most of the experimental work, and wrote the manuscript together. Yannan Wang, Li Zhang, Xiangong Chen and Xiaoping Yang did some experiments in this study. Haizheng Xiong, Gehendra Bhattarai, Waltram Ravelombola and Dotun Olaoye performed part bioinformatics analysis. Ainong Shi and Guohong Yang supervised and guided this research. All authors reviewed and approved the manuscript.

Declaration of competing interest

The authors declare that they have no known competing financial interests or personal relationships that could have appeared to influence the work reported in this paper.

Acknowledgements

The authors are thankful for the grants on this research supported by Earmarked Fund for China Agriculture Research System (grant number: CARS-10-C14), National Natural Science Foundation of China (grant number: U1404316) and China Scholarship Council (grant number: 201808410131).

Appendix A. Supplementary data

Supplementary data to this article can be found online at https://doi.org/10.1016/j.plaphy.2019.12.035.

Uncited reference

Ji-Min et al., 2011.

References

Brummell, D.A., Watson, L.M., Zhou, J., McKenzie, M.J., Hallett, I.C., Simmons, L., Carpenter, M., Timmerman-Vaughan, G.M., 2015. Overexpression of *STARCH BRANCHING ENZYME II* increases short-chain branching of amylopectin and alters the physicochemical properties of starch from potato tuber. BMC Biotechnol. 15, 28.

Castellarin, S.D., Pfeiffer, A., Sivilotti, P., Degan, M., Peterlunger, E., Gaspero, G.D., 2007. Transcriptional regulation of anthocyanin biosynthesis in ripening fruits of grapevine under seasonal water deficit. Plant Cell Environ. 30, 1381–1399.

Chen, H., Boutros, P.C., 2011. VennDiagram: a package for the generation of highly-customizable Venn and Euler diagrams in R. BMC Bioinf. 12, 35.

UNCORRECTED PROOF

Chen, Y.F., Li, L.Q., Xu, Q., Kong, Y.H., Wang, H., Wu, W.H., 2009. The WRKY6 transcription factor modulates *PHOSPHATE1* expression in response to low Pi stress in *Arabidopsis*. Plant Cell 21, 3554–3566.

Crevillén, P., Ventriglia, T., Pinto, F., Orea, A., Mérida, A., Romero, J.M., 2005. Differential pattern of expression and sugar regulation of *Arabidopsis thaliana* ADP-glucose pyrophosphorylase-encoding genes. J. Biol. Chem. 280, 8143–8149.

Curien, G., Giustini, C., Montillet, J.L., Mas-Y-Mas, S., Cobessi, D., Ferrer, J.L., Matringe, M., Grechkin, A., Rolland, N., 2016. The chloroplast membrane associated ceQORH putative quinone oxidoreductase reduces long-chain, stress-related oxidized lipids. Phytochemistry 122, 45–55.

Devaiah, B.N., Karthikeyan, A.S., Raghothama, K.G., 2007. WRKY75 transcription factor is a modulator of phosphate acquisition and root development in *Arabidopsis*. Plant Physiol 143, 1789–1801.

Devaiah, B.N., Raghothama, K.G., 2007. Transcriptional regulation of Pi starvation responses by WRKY75. Plant Signal. Behav. 2, 424–425.

Drapal, M., Rossel, G., Heider, B., Fraser, P.D., 2019. Metabolic diversity in sweet potato (*Ipomoea batatas* Lam.) leaves and storage roots. Hortic. Res. 6, 2.

Endrias, D., Negussie, R., Gulelat, D., 2016. Comparison of three sweet potato (*Ipomoea batatas* (L.) Lam) varieties on nutritional and anti-nutritional factors. Glob. J. Sci. Front. Res. (GJSFR) 16, 63–72.

Fekadu, G., Shimelis, H., Mark, L., 2013. Self- and cross-incompatibilities in sweetpotato and their implications on breeding. AJCS 7, 2074–2078.

Feller, A., Machemer, K., Braun, E.L., Grotewold, E., 2011. Evolutionary and comparative analysis of MYB and bHLH plant transcription factors. Plant J. 66, 94–116.

Gonzalez, A., Zhao, M., Leavitt, J.M., Lloyd, A.M., 2008. Regulation of the anthocyanin biosynthetic pathway by the TTG1/bHLH/Myb transcriptional complex in Arabidopsis seedlings. Plant J. 53, 814–827.

Grabherr, M.G., Haas, B.J., Yassour, M., Levin, J.Z., Thompson, D.A., Amit, I., Adiconis, X., Fan, L., Raychowdhury, R., Zeng, Q., Chen, Z., Mauceli, E., Hacohen, N., Gnirke, A., Rhind, N., di Palma, F., Birren, B.W., Nusbaum, C., Lindblad-Toh, K., Friedman, N., Regev, A., 2011. Full-length transcriptome assembly from RNA-Seq data without a reference genome. Nat. Biotechnol. 29, 644–652.

Harborne, J.B., Williams, C.A., 2000. Advances in flavonoid research since 1992. Phytochemistry 55, 481–504.

Ingabire, M.R., Hilda, V., 2011. Comparison of the nutrient composition of four sweet potato varieties cultivated in Rwanda. Am. J. Food Nutr. 1, 34–38.

Jiang, H., Lei, R., Ding, S.W., Zhu, S., 2014. Skewer: a fast and accurate adapter trimmer for next-generation sequencing paired-end reads. BMC Bioinf. 15, 182.

Ji-Min, S., Bong-Kyu, K., Sang-Gyu, S., Seo, B.J., Ji-Seong, K., Byung-ki, J., Si-Yong, K., Joon-Seol, L., Mi-Nam, C., Sun-Hyung, K., 2011. Mutation breeding of sweet potato by gamma-ray radiation. Afr. J. Agric. Res. 6, 1447–1454.

Katayama, K., Kobayashi, A., Sakai, T., Kuranouchi, T., Kai, Y., 2017. Recent progress in sweetpotato breeding and cultivars for diverse applications in Japan. Breed Sci. 67, 3–14.

Kiferle, C., Fantini, E., Bassolino, L., Povero, G., Spelt, C., Buti, S., Giuliano, G., Quattrocchio, F., Koes, R., Perata, P., Gonzali, S., 2015. Tomato R2R3-MYB proteins SlANT1 and SlAN2: same protein activity, different roles. PLoS One 10, e0136365.

Kim, S., Hwang, G., Lee, S., Zhu, J.Y., Paik, I., Nguyen, T.T., Kim, J., Oh, E., 2017. High ambient temperature represses anthocyanin biosynthesis through degradation of HY5. Front. Plant Sci. 8, 1787.

Kou, M., Liu, Y.J., Li, Z.Y., Zhang, Y.G., Tang, W., Yan, H., Wang, X., Chen, X.G., Su, Z.X., Arisha, M.H., Li, Q., Ma, D.F., 2019. A novel glutathione S-transferase gene from sweetpotato, *IbGSTF4*, is involved in anthocyanin sequestration. Plant Physiol. Biochem. 135, 395–403.

Langfelder, P., Horvath, S., 2008. WGCNA: an R package for weighted correlation network analysis. BMC Bioinf. 9, 559.

Lei, L., Li, Y., Wang, Q., Xu, J., Chen, Y., Yang, H., Ren, D., 2014. Activation of MKK9-MPK3/MPK6 enhances phosphate acquisition in *Arabidopsis thaliana*. New Phytol. 203, 1146–1160.

Leyva, A., Jarillo, J.A., Salinas, J., Martinez-Zapater, J.M., 1995. Low temperature induces the accumulation of *Phenylalanine Ammonia-Lyase* and *Chalcone Synthase* mRNAs of *Arabidopsis thaliana* in a light-dependent manner. Plant Physiol 108, 39–46.

Li, W., Godzik, A., 2006. Cd-hit: a fast program for clustering and comparing large sets of protein or nucleotide sequences. Bioinformatics 22, 1658–1659.

Lin-Wang, K., Micheletti, D., Palmer, J., Volz, R., Lozano, L., Espley, R., Hellens, R.P., Chagnè, D., Rowan, D.D., 2011. Troggio M, Iglesias I, Allan AC. High temperature reduces apple fruit colour via modulation of the anthocyanin regulatory complex. Plant Cell Environ. 34, 1176–1190.

Liu, Q.C., 2011. Sweet potato omics and biotechnology in China. Plant Omics J 4, 295–301.

Liu, Q.C., 2017. Improvement for agronomically important traits by gene engineering in sweetpotato. Breed Sci. 67, 15–26.

Liu, Y., Lin-Wang, K., Espley, R.V., Wang, L., Li, Y., Liu, Z., Zhou, P., Zeng, L., Zhang, X., Zhang, J., Allan, A.C., 2019. StMYB44 negatively regulates anthocyanin biosynthesis at high temperatures in tuber flesh of potato. J. Exp. Bot. 70, 3809–3824.

Liu, Z., Jia, Y., Ding, Y., Shi, Y., Li, Z., Guo, Y., Gong, Z., Yang, S., 2017. Plasma membrane CRPK1-mediated phosphorylation of 14-3-3 proteins induces their nuclear import to fine-tune CBF signaling during cold response. Mol. Cell 66, 117–128.

Lloyd, A., Brockman, A., Aguirre, L., Campbell, A., Bean, A., Cantero, A., Gonzalez, A., 2017. Advances in the MYB-bHLH-WD repeat (MBW) pigment regulatory model: addition of a WRKY factor and co-option of an anthocyanin MYB for betalain regulation. Plant Cell Physiol. 58, 1431–1441.

Love, M.I., Huber, W., Anders, S., 2014. Moderated estimation of fold change and dispersion for RNA-seq data with DESeq2. Genome Biol. 15, 550.

Lu, W., Tang, X., Huo, Y., Xu, R., Qi, S., Huang, J., Zheng, C., Wu, C.A., 2012. Identification and characterization of fructose 1,6-bisphosphate aldolase genes in *Arabidopsis* reveal a gene family with diverse responses to abiotic stresses. Gene 503, 65–74.

Mahmood, K., Xu, Z., El-Kereamy, A., Casaretto, J.A., Rothstein, S.J., 2016. The *Arabidopsis* transcription factor ANAC032 represses anthocyanin biosynthesis in response to high sucrose and oxidative and abiotic stresses. Front. Plant Sci. 7, 1548.

Ma, P., Bian, X., Jia, Z., Guo, X., Xie, Y., 2016. De novo sequencing and comprehensive analysis of the mutant transcriptome from purple sweet potato (*Ipomoea batatas* L.). Gene 575, 641–649.

Moore, B., Zhou, L., Rolland, F., Hall, Q., Cheng, W.H., Liu, Y.X., Hwang, I., Jones, T., Sheen, J., 2003. Role of the *Arabidopsis* glucose sensor HXK1 in nutrient, light, and hormonal signaling. Science 300, 332–336.

Morishita, T., Kojima, Y., Maruta, T., Nishizawa-Yokoi, A., Yabuta, Y., Shigeoka, S., 2009. Arabidopsis NAC transcription factor, ANAC078, regulates flavonoid biosynthesis under high-light. Plant Cell Physiol. 50, 2210–2222.

Mousley, C.J., Tyeryar, K.R., Ryan, M.M., Bankaitis, V.A., 2006. Sec14p-like proteins regulate phosphoinositide homoeostasis and intracellular protein and lipid trafficking in yeast. Biochem. Soc. Trans. 34, 346–350.

Nakabayashi, R., Yonekura-Sakakibara, K., Urano, K., Suzuki, M., Yamada, Y., Nishizawa, T., Matsuda, F., Kojima, M., Sakakibara, H., Shinozaki, K., Michael, A.J., Tohge, T., Yamazaki, M., Saito, K., 2014. Enhancement of oxidative and drought tolerance in Arabidopsis by overaccumulation of antioxidant flavonoids. Plant J. 77, 367–379.

Noman, A., Aqeel, M., Deng, J., Khalid, N., Sanaullah, T., Shuilin, H., 2017. Biotechnological advancements for improving floral attributes in ornamental plants. Front. Plant Sci. 8, 530.

Noda, Y., Yamagishi, T., Yoda, K., 2007. Specific membrane recruitment of Uso1 protein, the essential endoplasmic reticulum-to-Golgi tethering factor in yeast vesicular transport. J. Cell. Biochem. 101, 686–694.

Oracion, M.Z., Niwa, K., Shiotani, I., 1990. Cytological analysis of tetraploid hybrids between sweet potato and diploid *Ipomoea trifida* (H. B. K.) Don. Theor. Appl. Genet. 80, 617–624.

Patro, R., Duggal, G., Love, M.I., Irizarry, R.A., Kingsford, C., 2017. Salmon provides fast and bias-aware quantification of transcript expression. Nat. Methods 14, 417–419.

Patterson, J.A., Tetlow, I.J., Emes, M.J., 2018. Bioinformatic and *in vitro* analyses of Arabidopsis starch synthase 2 reveal post-translational regulatory mechanisms. Front. Plant Sci. 9, 1338.

Pei, J., Wang, H., Xia, Z., Liu, C., Chen, X., Ma, P., Lu, C., Wang, W., 2015. Phylogeny and expression pattern of starch branching enzyme family genes in cassava (*Manihot esculenta* Crantz) under diverse environments. Mol. Cell. Biochem. 406, 273–284.

Qiu, Z., Wang, X., Gao, J., Guo, Y., Huang, Z., Du, Y., 2016. The tomato *Hoffman's Anthocyaninless* gene encodes a bHLH transcription factor involved in anthocyanin biosynthesis that is developmentally regulated and induced by low temperatures. PLoS One 11, e0151067.

Rodrigues-Amaya, D.B., Kimura, M., 2004. Harvestplus Handbook for Carotenoid Analysis. HarvestPlus Technical Monograph 2. IFPRI and CIAT, Washington DC and Cali.

Solfanelli, C., Poggi, A., Loreti, E., Alpi, A., Perata, P., 2006. Sucrose-specific induction of the anthocyanin biosynthetic pathway in *Arabidopsis*. Plant Physiol 140, 637–646.

Šulc, M., Kotíková, Z., Paznocht, L., Pivec, V., Hamouz, K., Lachman, J., 2017. Changes in anthocyanidin levels during the maturation of color-fleshed potato (*Solanum tuberosum* L.) tubers. Food Chem. 237, 981–988.

Tanaka, M., Ishiguro, K., Oki, T., Okuno, S., 2017. Functional components in sweetpotato and their genetic improvement. Breed Sci. 67, 52–61.

Teng, S., Keurentjes, J., Bentsink, L., Koornneef, M., Smeekens, S., 2005. Sucrose-specific induction of anthocyanin biosynthesis in Arabidopsis requires the MYB75/PAP1 gene. Plant Physiol 139, 1840–1852.

Teow, C.C., Truong, V.D., McFeeters, R.F., Thomopson, R.L., Pecota, K.V., Yencho, G.C., 2007. Antioxidant activities, phenolic and β-carotene contents of sweet potato genotypes with varying flesh colours. Food Chem. 103, 829–838.

Tian, Q., Konczak, I., Schwartz, S.J., 2005. Probing anthocyanin profiles in purple sweet potato cell line (*Ipomoea batatas* L. Cv. Ayamurasaki) by high-performance liquid chromatography and electrospray ionization tandem mass spectrometry. J. Agric. Food Chem. 53, 6503–6509.

Timothy, A.H., Edwina, C.C., 1995. Genetics and biochemistry of ant hocyanin biosynthesis. Plant Cell 7, 1071–1083.

Velu, S., Oleg, F., Sonia, D., Ben, W., Noam, A., 2016. Increased anthocyanin and flavonoids in mango fruit peel are associated with cold and pathogen resistance. Postharvest Biol. Technol. 111, 132–139.

Verweij, W., Spelt, C.E., Bliek, M., de Vries, M., Wit, N., Faraco, M., Koes, R., Quattrocchio, F.M., 2016. Functionally similar WRKY proteins regulate vacuolar acidification in petunia and hair development in Arabidopsis. Plant Cell 28, 786–803.

Wang, A., Li, R., Ren, L., Gao, X., Zhang, Y., Ma, Z., Ma, D., Luo, Y., 2018. A comparative metabolomics study of flavonoids in sweet potato with different flesh colors (*Ipomoea batatas* (L.) Lam). Food Chem. 260, 124–134.

Wang, J., Lian, W., Cao, Y., Wang, X., Wang, G., Qi, C., Liu, L., Qin, S., Yuan, X., Li, X., Ren, S., Guo, Y.D., 2018. Overexpression of *BoNAC019*, a NAC transcription factor from *Brassica oleracea*, negatively regulates the dehydration response and anthocyanin biosynthesis in *Arabidopsis*. Sci. Rep. 8, 13349.

Wang, P., Richardson, C., Hawkins, T.J., Sparkes, I., Hawes, C., Hussey, P.J., 2016. Plant VAP27 proteins: domain characterization, intracellular localization and role in plant development. New Phytol. 210, 1311–1326.

Wang, S., Pan, D., Lv, X., Song, X., Qiu, Z., Huang, C., Huang, R., Chen, W., 2016. Proteomic approach reveals that starch degradation contributes to anthocyanin accumulation in tuberous root of purple sweet potato. J Proteom 143, 298–305.

Wang, Y.P., Wang, F., Zhai, H., Liu, Q.C., 2007. Production of a useful mutant by chronic irradiation in sweetpotato. Sci. Hortic. 111, 173–178.

UNCORRECTED PROOF

Wu, A., Allu, A.D., Garapati, P., Siddiqui, H., Dortay, H., Zanor, M.I., Asensi-Fabado, M.A., Munné-Bosch, S., Antonio, C., Tohge, T., Fernie, A.R., Kaufmann, K., Xue, G.P., Mueller-Roeber, B., Balazadeh, S., 2012. *JUNGBRUNNEN1*, a reactive oxygen species-responsive NAC transcription factor, regulates longevity in Arabidopsis. Plant Cell 24, 482–506.

Yang, Y., Shi, D., Wang, Y., Yang, G., Xu, X., Zhai, H., He, S., Liu, Q., Su, W., 2017. Development and cluster analysis of SSR markers based on transcriptional sequencing data of sweetpotato. Mol. Plant Breed. 16, 3569–3579. (In Chinese).

Yang, Y., Wang, Y., Jia, L., Yang, G., Xu, X., Zhai, H., He, S., Li, J., Dai, X., Qin, N., Zhu, C., Liu, Q., 2018. Involvement of an ABI-like protein and a Ca^{2+}-ATPase in drought tolerance as revealed by transcript profiling of a sweetpotato somatic hybrid and its parents *Ipomoea batatas* (L.) Lam. and *I. triloba* L. PLoS One 13, e0193193.

Yoshinaga, M., Yamakawa, O., Nakatani, M., 1999. Genotypic diversity of anthocyanin content and composition in purple-fleshed sweet potato (*Ipomoea batatas* (L.) Lam). Breed Sci. 49, 43–47.

Zeeman, S.C., Kossmann, J., Smith, A.M., 2010. Starch: its metabolism, evolution, and biotechnological modification in plants. Annu. Rev. Plant Biol. 61, 209–234.

Zhang, B., Horvath, S., 2005. A general framework for weighted gene co-expression network analysis. Stat. Appl. Genet. Mol. Biol. 4, 17. Art.

Zhang, N., Sun, Q., Li, H., Li, X., Cao, Y., Zhang, H., Li, S., Zhang, L., Qi, Y., Ren, S., Zhao, B., Guo, Y.D., 2016. Melatonin improved anthocyanin accumulation by regulating gene expressions and resulted in high reactive oxygen species scavenging capacity in cabbage. Front. Plant Sci. 7, 197.

Zhang, X., Szydlowski, N., Delvallé, D., D'Hulst, C., James, M.G., Myers, A.M., 2008. Overlapping functions of the starch synthases SSII and SSIII in amylopectin biosynthesis in *Arabidopsis*. BMC Plant Biol. 8, 96.

Zhao, J., Dixon, R.A., 2010. The 'ins' and 'outs' of flavonoid transport. Trends Plant Sci. 15, 72–80.

Zhao, J., 2015. Flavonoid transport mechanisms: how to go, and with whom. Trends Plant Sci. 20, 576–585.

Zheng, Y., Tian, L., Liu, H., Pan, Q., Zhan, J., Huang, W., 2009. Sugars induce anthocyanin accumulation and flavanone 3-hydroxylase expression in grape berries. Plant Growth Regul. 58, 251–260.

Zhu, H., Qian, W., Lu, X., Li, D., Liu, X., Liu, K., Wang, D., 2005. Expression patterns of purple acid phosphatase genes in *Arabidopsis* organs and functional analysis of *AtPAP23* predominantly transcribed in flower. Plant Mol. Biol. 59, 581–594.

UNCORRECTED PROOF